

Magnetic couplings, optical spectra, and spin-orbit exciton in 5d electron Mott insulator Sr₂IrO₄

Beom Hyun Kim¹, G. Khaliullin², and B. I. Min^{1*}

¹*Department of Physics, PCTP, Pohang University of Science and Technology, Pohang 790-784, Korea and*

²*Max Planck Institute for Solid State Research, Heisenbergstrasse 1, D-70569 Stuttgart, Germany*

(Dated: August 14, 2018)

Based on the microscopic model including spin-orbit coupling, on-site Coulomb and Hund's interactions, as well as crystal field effects, we have investigated magnetic and optical properties of Sr₂IrO₄. Taking into account all intermediate state multiplets generated by virtual hoppings of electrons, we calculated the isotropic, pseudodipolar, and Dzyaloshinsky-Moriya coupling constants, which describe the experiment quite well. The optical conductivity $\sigma(\omega)$ evaluated by the exact diagonalization method shows two peaks at ~ 0.5 and ~ 1.0 eV in agreement with experiment. The two peak structure of $\sigma(\omega)$ arises from the unusual Fano-type overlap between electron-hole continuum of the $J_{eff} = 1/2$ band and the intrasite spin-orbit exciton observed recently in Sr₂IrO₄.

PACS numbers: 75.30.Et, 71.70.Ej, 78.20.Bh

Mott physics is one of the most fundamental phenomena in condensed matter physics giving rise to diverse and fascinating collective behavior of correlated electrons [1]. In Mott insulators, strong on-site Coulomb repulsion (U) splits the half-filled band into the lower Hubbard band (LHB) accommodating the spin and orbital degrees of freedom of electrons, and the empty upper Hubbard bands (UHB). The electrons hop into adjacent sites only virtually, overcoming thereby the Mott-Hubbard gaps. Typically, the antiferromagnetic (AFM) ground state is realized due to the kinetic energy gain of the virtual exchange processes. The optical conductivity shows peak structures at the absorption edges corresponding to the transitions between LHB and UHBs.

Recently, a new class of 5d Mott insulators such as Sr₂IrO₄ [2–4] and Na₂IrO₃ [5, 6] has been discovered, where the strong spin-orbit (SO) coupling is crucial for stabilizing the insulating state. The Coulomb interaction between 5d-electrons $U \sim 2$ eV is much smaller than that in conventional 3d electron Mott insulators. On the other hand, the SO coupling $\lambda \simeq 0.4$ eV in iridates is much larger and splits ${}^2T_{1g}$ states of 5d⁵-shell into the half-filled $J_{eff} = 1/2$ and fully-occupied $J_{eff} = 3/2$ states. Then the narrow $J_{eff} = 1/2$ band tends to undergo Mott transition even at relatively small U [2, 3, 7–9].

The issue in iridates is to which extent the physical properties and model descriptions of $J_{eff} = 1/2$ systems are (dis)similar to those of conventional 3d Mott insulators. The best studied member of 5d Mott systems is Sr₂IrO₄ perovskite. Its in-plane canted AFM ground state [4], magnon spectra [S5], and finite temperature spin dynamics [11] closely resemble those of parent high- T_c cuprates, in accord with the theoretical predictions [12] based on Mott-Hubbard picture. In addition to magnons, resonant inelastic x-ray scattering (RIXS) experiments [13, S5] have observed also the higher energy broad peak at $\sim 0.5 - 0.8$ eV. Based on the theoretical expectations [12, 14, 15] that the SO split t_{2g} man-

ifold should have a magnetically active mode at $\sim \frac{3}{2}\lambda$, this peak has been attributed to the transition between $J_{eff} = 1/2$ and $3/2$ states and termed “SO exciton” [S5].

Concerning the charge excitation spectra, the optical conductivity $\sigma(\omega)$ of Sr₂IrO₄ shows two peaks at ~ 0.5 and ~ 1.0 eV [2] that are preserved up to high temperatures [16]. The first peak was assigned to the transition from occupied $J_{eff} = 1/2$ LHB to $J_{eff} = 1/2$ UHB, while the peak at ~ 1.0 eV to that from $J_{eff} = 3/2$ to unoccupied $J_{eff} = 1/2$ [2]. This interpretation, however, is based on a picture of single-electron density of states. In fact, there has been no theoretical calculations of $\sigma(\omega)$ in iridates taking into account the many-electron multiplet structure of excited states, which is known to be essential for the interpretation of optical data. Moreover, there are inherent relations between the optical absorption peaks/intensities and the strength of magnetic couplings (both are determined by the same virtual hoppings and excited multiplets), which enable one to extract the physical parameters, such as U and Hund's coupling J_H , from a combined analysis of the magnetic and optical data [17–19]. The aim of the present Letter is to extend this fruitful approach to the 5d electron Mott insulators.

We have calculated the magnetic couplings, optical conductivity, and RIXS spectra in Sr₂IrO₄ by exact diagonalization (ED) of a microscopic model on small clusters, fully incorporating the multiplet structure of Ir ions, SO coupling, tetragonal distortion, and octahedral rotations. The magnetic couplings obtained are consistent with the available data [4, 11, S5]. Calculated RIXS spectra reproduce the SO exciton mode. More interestingly, we found that, unlike the case of 3d oxides [17–19], the observed peaks in $\sigma(\omega)$ of Sr₂IrO₄ cannot be directly determined from the multiplet energies and intensities. Instead, the strong mixing between intersite optical excitations (electron-hole continuum) and intraionic transition between $J_{eff} = 1/2$ and $3/2$ states (SO exciton) is found to be essential feature of Sr₂IrO₄. This implies that nei-

ther purely atomic nor simple band picture is sufficient to describe the small charge-gap iridium oxides.

Model.— To describe the electronic structure of Ir ions, we adopted the following Hamiltonian:

$$H_{ion} = \sum_{\tau\tilde{\sigma}} \epsilon_{\tau} n_{\tau\tilde{\sigma}} + \frac{1}{2} \sum_{\sigma\sigma'\mu\nu} U_{\mu\nu} c_{\mu\sigma}^{\dagger} c_{\nu\sigma'}^{\dagger} c_{\nu\sigma'} c_{\mu\sigma} \quad (1)$$

$$+ \frac{1}{2} \sum_{\substack{\sigma\sigma' \\ \mu\neq\nu}} J_{\mu\nu} c_{\mu\sigma}^{\dagger} c_{\nu\sigma'}^{\dagger} c_{\mu\sigma'} c_{\nu\sigma} + \frac{1}{2} \sum_{\substack{\sigma \\ \mu\neq\nu}} J'_{\mu\nu} c_{\mu\sigma}^{\dagger} c_{\mu-\sigma}^{\dagger} c_{\nu-\sigma} c_{\nu\sigma},$$

where τ and isospin $\tilde{\sigma}$ [12] refer to the lowest three Kramers doublets [the eigenstates in the presence of the tetragonal crystal field splitting Δ_{xy} and SO coupling, see Fig. 1(a)]. The other terms describe the on-site Coulomb and Hund's interactions, where μ and σ are the orbital and spin indices, respectively. As usual, we parametrize the interaction matrix as $U_{\mu\mu} = U$, $U_{\mu\neq\nu} = U - 2J_H$, and $J_{\mu\nu} = J'_{\mu\nu} = J_H$ [20].

Fig. 1(b,c) shows all possible multiplets of d^5 and d^4 electronic configurations. For d^6 , all three lowest Kramers doublets $\tau_{1,2,3}$ are fully occupied. We note that the wave-functions of these states are often taken in the limit of $10Dq \rightarrow \infty$, i.e., admixture of e_g orbitals ($\propto \lambda/10Dq$) in the ground state via SO coupling is ignored. Since the SO coupling in iridates is strong, we fully include the e_g orbital admixture in the lowest Kramers doublets.

Because an electron hops between nearest-neighbor (NN) Ir sites via an oxygen [see Fig. 1(d)], and the charge transfer energy Δ between Ir-5d and O-2p is large ($\Delta \sim 3.3$ eV [22]), we assumed the following effective NN hopping Hamiltonian:

$$H_{ij} = \sum_{\tau\tau'\tilde{\sigma}\tilde{\sigma}'} \left(t_{i\tau\tilde{\sigma};j\tau'\tilde{\sigma}'} c_{j\tau'\tilde{\sigma}'}^{\dagger} c_{i\tau\tilde{\sigma}} + h.c. \right), \quad (2)$$

where the effective hopping integral between $\tau\tilde{\sigma}$ and $\tau'\tilde{\sigma}'$ states is $t_{i\tau\tilde{\sigma};j\tau'\tilde{\sigma}'} = \sum_{p\sigma} \frac{t_{i\tau\tilde{\sigma};p\sigma} t_{j\tau'\tilde{\sigma}';p\sigma}^*}{\sqrt{(\Delta+\epsilon_{\tau})(\Delta+\epsilon_{\tau'})}}$. We calculated the pd -hopping matrix $t_{i\tau\tilde{\sigma};p\sigma}$ between $5d$ Ir and $2p$ O orbitals in terms of two parameters $t_{pd\sigma}$ and $t_{pd\pi}$ [23].

Magnetic interactions.— We considered the Ir₁-Ir₂ pair described by the following Hamiltonian:

$$H = H_1 + H_2 + H_{12}. \quad (3)$$

Here H_1 and H_2 are the ionic Hamiltonians given by Eq. (1), and H_{12} is the hopping term of Eq. (2). Using the ED method, we solved this Hamiltonian numerically, taking into account all possible multiplets allowed for the $d^5 - d^5$ and $d^4 - d^6$ configurations, and

TABLE I: Physical parameters in units of eV.

$10Dq$	Δ	Δ_{xy}	U	J_H	λ	$t_{pd\sigma}$	$t_{pd\pi}$
3.0	3.3	0.15	1.86	0.5	0.4	-1.8	0.83

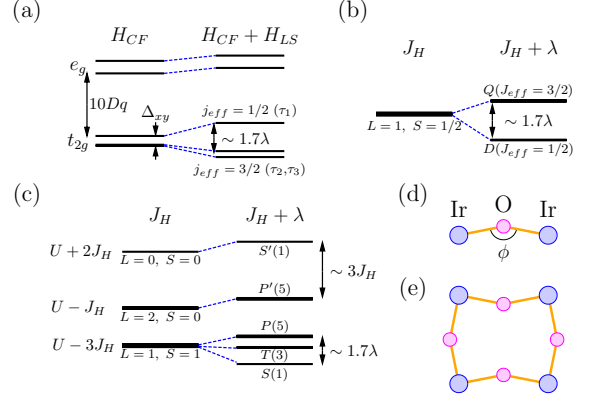


FIG. 1: (color online) (a) Energy levels of d electron in the presence of the cubic crystal field $10Dq$, the tetragonal crystal field Δ_{xy} , and the SO interaction λ [21]. The lowest multiplet levels of (b) d^5 and (c) d^4 configurations including SO λ and the Hund's coupling J_H . (d) Two-site and (e) four-site clusters in the xy -plane, which were employed in the evaluation of the magnetic couplings and conductivity $\sigma(\omega)$.

obtained eigenvalues E_n and eigenstates $|\psi_n\rangle$ of the Ir-Ir cluster. The Hamiltonian can be then expressed as $H = \sum_n E_n |\psi_n\rangle \langle \psi_n|$. Without the hopping term H_{12} , the Ir-Ir pair would have four degenerate states denoted by $|\psi_i^0\rangle$ ($i = 1-4$). The magnetic interactions are generated by virtual hoppings among them. The resulting effective magnetic Hamiltonian can be obtained by applying the projection operator $\mathcal{P}_{1/2} = \sum_{i=1}^4 |\psi_i^0\rangle \langle \psi_i^0|$ onto H [24]:

$$\mathcal{P}_{1/2} H \mathcal{P}_{1/2} - \frac{1}{4} \text{Tr} (\mathcal{P}_{1/2} H \mathcal{P}_{1/2}) = \tilde{\mathbf{S}}_1 \cdot \mathcal{J} \cdot \tilde{\mathbf{S}}_2, \quad (4)$$

where $\tilde{\mathbf{S}}$ is isospin one-half, and \mathcal{J} is a 3×3 tensor.

Consistent with symmetry considerations as well as with Ref. [12], we found that Eq. (4) comprises four distinct nonvanishing terms,

$$J \tilde{\mathbf{S}}_1 \cdot \tilde{\mathbf{S}}_2 + \delta J_z \tilde{S}_{1,z} \tilde{S}_{2,z} + \delta J_{xy} (\tilde{\mathbf{S}}_1 \cdot \tilde{\mathbf{r}}_{12}) (\tilde{\mathbf{S}}_2 \cdot \tilde{\mathbf{r}}_{12}) + \mathbf{D} \cdot \tilde{\mathbf{S}}_1 \times \tilde{\mathbf{S}}_2, \quad (5)$$

corresponding to isotropic Heisenberg (J), symmetric (δJ_z , δJ_{xy}) and antisymmetric (\mathbf{D}) anisotropic couplings between NN Ir-moments. We note that only the z -component Dzyaloshinsky-Moriya (DM) vector \mathbf{D} survives because of the mirror symmetry with respect to the xy -plane, i.e., $\mathbf{D} = (0, 0, D)$.

Figure 2 presents the magnetic coupling constants, calculated by using the parameters provided in Table I, as a function of Ir-O-Ir bonding angle ϕ . $10Dq$ and Δ values are adopted from Refs. [13, 22, 25] and λ from Refs. [25, 26]. We have determined the optimal values of U , J_H , t_{pd} such that they describe both the magnetic and optical data properly [27]. We set tetragonal splitting $\Delta_{xy} = 0.15$ eV; at this value, $|D/J|$ ratio becomes $\simeq 0.34$ and yields the spin canting angle of $\simeq 9.3^\circ$ at $\phi = 158^\circ$ (as in Sr₂IrO₄). As shown in the inset of Fig. 2,

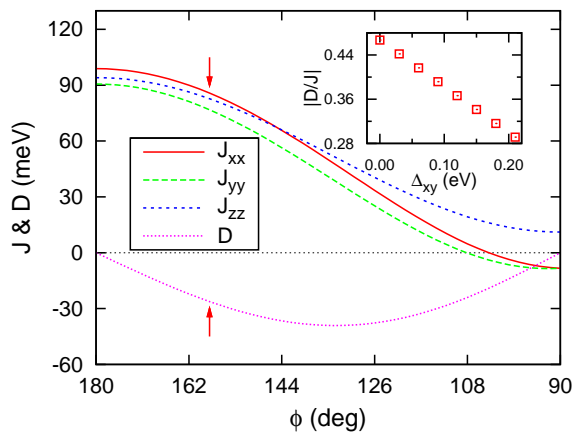


FIG. 2: (color online) Magnetic coupling constants between NN Ir ions ($\vec{r}_{12}||x$) with respect to the bonding angle (ϕ). J_{xx} , J_{yy} , and J_{zz} represent diagonal parts of the superexchange tensor \mathcal{J} . $J_{xx} = J + \delta J_{xy}$, $J_{yy} = J$, and $J_{zz} = J + \delta J_z$ are deduced from Eq. (5). D is a z -component of the DM vector \mathbf{D} . Arrows denote the bonding angle in Sr_2IrO_4 . Inset shows $|D/J|$ ratio as a function of the tetragonal splitting Δ_{xy} .

when Δ_{xy} is too small, $|D/J|$ ratio becomes too large to describe the observed spin canting. Approximately, we find that $D \propto \sin(2\phi)$. The spin canting angle of $\sim 9.3^\circ$ is close to those found in previous studies [12, 28]. Noteworthy is that the Ising coupling $\delta J_z (= J_{zz} - J_{yy})$ in Eq. (5) is enhanced when decreasing bonding angle ϕ . We also calculated a pseudodipolar coupling δJ_{xy} for different J_H values and found that δJ_{xy} becomes zero at $J_H = 0$. Both of these observations agree with the analytical results [12].

Summarizing our results for magnetic interactions in Sr_2IrO_4 , we obtained the following values at $\phi = 158^\circ$: $J \simeq 76.8$, $D \simeq -26.2$, $\delta J_z \simeq 5.9$, and $\delta J_{xy} \simeq 8.6$ meV. With these coupling constants, the interactions of Eq. (5) lead to the canted AFM state with Ir-moments lying in the xy -plane, as observed in Sr_2IrO_4 [4]. The calculated isotropic coupling J is in close agreement with the experimental value of $J \simeq 60$ meV [S5]. Unusually large anisotropic couplings $D, \delta J_z, \delta J_{xy}$ found here are the direct fingerprints of strong SO interaction.

Optical conductivity and RIXS spectra.— In 3d Mott insulators, the hopping between NN sites plays a dominant role in $\sigma(\omega)$ that shows peak structures near the ionic multiplet states $d_i^{n-1} - d_j^{n+1}$ [17–19], and 2-site cluster may capture essential features of $\sigma(\omega)$. In contrast, 5d Mott insulators have weaker Coulomb repulsion and thus a duality of atomic and band nature of correlated electrons is more pronounced [S5]. In order to capture the delocalization of optically excited electron-hole (e-h) pairs, we consider here a 2×2 cluster shown in Fig. 1(e).

We considered all possible multiplets within the d^5 - d^5 - d^5 - d^5 and d^4 - d^6 - d^5 - d^5 charge configurations. In order to

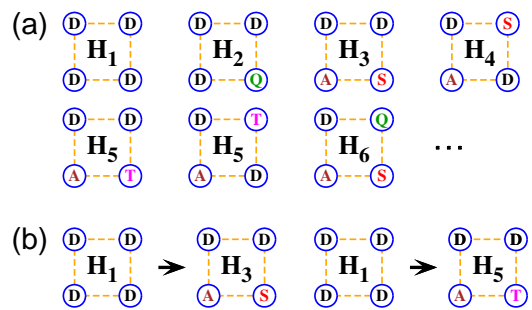


FIG. 3: (color online) (a) Schematic diagrams of possible multiplets included in subsets (\mathbf{H}_i) of the Hilbert space. D , Q , S , and T refer to multiplets of d^5 and d^4 , as labeled in Fig. 1(b) and (c), and A denotes a nondegenerate d^6 state. \mathbf{H}_5 includes also diagrams (not shown) with P, P', S' multiplets of the d^4 state [Fig. 1(c)]. (b) Two examples of optically active transitions that contribute to $\sigma(\omega)$ at low energies. The final states \mathbf{H}_3 and \mathbf{H}_5 have an overlap with on-site local SO exciton Q (i.e., with \mathbf{H}_2 sector), due to intersite hoppings between $J_{eff} = 1/2$ and $J_{eff} = 3/2$ states, resulting in two peak structure of $\sigma(\omega)$.

clarify the origin of optical peaks, it is useful to classify the Hilbert space into 6 subspaces [see Fig. 3(a)]: \mathbf{H}_1 of four d^5 doublets (D), \mathbf{H}_2 of one or more quartets (Q) among four d^5 configurations, \mathbf{H}_3 of two D 's of d^5 and NN e-h pairs $d^4(S)-d^6(A)$, \mathbf{H}_4 of two D 's of d^5 and next nearest-neighbor (NNN) e-h pairs $d^4(S)-d^6(A)$, \mathbf{H}_5 of two D 's of d^5 and (NN & NNN) e-h pairs $d^4(T, P, P', S')-d^6(A)$, and the remaining states (\mathbf{H}_6, \dots) that involve, e.g., simultaneous intersite e-h transitions and local SO exciton Q . All the above configurations couple to each other via the hopping Hamiltonian of Eq. (2).

We have solved the Hamiltonian matrix with the ED method, and obtained $\sigma(\omega)$ from the following relation:

$$\sigma(\omega) = \pi v \frac{1 - e^{-\beta\omega}}{\omega} \sum_{n < m} p_n |\langle \psi_m | \hat{J}_c | \psi_n \rangle|^2 \delta(\omega + E_n - E_m), \quad (6)$$

where v is volume per Ir-site, p_n is the probability density of eigenstate $|\psi_n\rangle$, and \hat{J}_c is the current operator. We set $\beta^{-1} = k_B T = 30$ meV to avoid the finite size effect. A function $\delta(\omega)$ is treated with broadening of 0.05 eV.

Figure 4(a) shows the result for $\sigma(\omega)$ calculated by using the parameters from Table I. Two peaks are revealed clearly at ~ 0.5 and ~ 1.0 eV, in good agreement with experiment. Estimated value of $\sigma(\omega)$ at ~ 0.5 eV is also consistent with the experimental data. For $\omega > 0.6$ eV, calculated $\sigma(\omega)$ is smaller than that observed. The possible reasons for this discrepancy are the contributions from the pd -charge transfer peak at ~ 3 eV and from two or more e-h pair excitations not included here.

Shown in Figure 4(b) is the RIXS spectra, calculated by employing the inelastic x-ray scattering operator of Ref. [15] instead of \hat{J}_c in Eq. (6). At the L_3 -edge, intense magnon (below 0.25 eV) and SO exciton (0.5 – 1.0 eV)

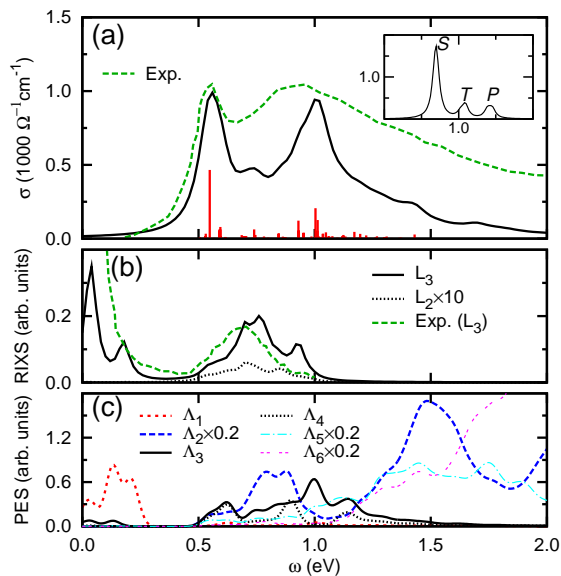


FIG. 4: (color online) (a) Optical conductivity calculated (solid line) and experimental data [2] (dashed line). Red vertical sticks show relative strengths and positions of optical transitions without broadening. Inset: the result for $\sigma(\omega)$ when the eigenstates $|\psi_n\rangle$ and energies E_n in Eq. (6) are approximated by purely local ionic multiplets. (b) Calculated L_3 -edge (solid line) and $10 \times L_2$ -edge (dotted line) RIXS spectra at $\mathbf{q} = (\pi, \pi)$. Dashed line: experimental data [S5]. (c) Projected excitation spectra: Λ_1 represents magnon band, Λ_2 contains one or more SO excitons, Λ_3 and Λ_4 represent NN and more distantly separated e-h excitations derived from the $J_{eff} = 1/2$ states, respectively, and Λ_5 shows the e-h continuum of $J_{eff} = 3/2$ states. Λ_6 refers to other excitations, e.g., simultaneous transitions in e-h and SO exciton channels.

bands are obtained, while the intensity at the L_2 -edge is nearly vanishing, in agreement with experiments [13, S5].

Of particular interest is the origin of two peaks in $\sigma(\omega)$ and their relation to SO exciton. In $3d$ Mott insulators, each peak would correspond to the specific multiplet of $d^{n-1} - d^{n+1}$ with the spectral weight proportional to $|\langle d^{n-1} d^{n+1} | J_c | d^n d^n \rangle|^2$ [17–19]. Such a simple ionic multiplet picture, however, is incomplete in iridates. Indeed, as shown in inset of Fig. 4(a), $\sigma(\omega)$ based on this picture shows that the first peak [$|DDDD\rangle \rightarrow |ASDD\rangle$ transition in Fig. 3(b)] is much stronger than those corresponding to higher energy transitions involving T, P -multiplets [29], in contrast to the observation that the spectral weight of ~ 1.0 eV peak is even larger than that of ~ 0.5 eV peak [Fig. 4(a)].

To understand how the e-h delocalization effects lead to strong deviations from a simple ionic picture, it is instructive to analyze the underlying excitation spectra in more detail. To this end, we evaluated the projected excitation spectrum (PES) of the 2×2 cluster into the subspaces \mathbf{H}_i introduced above:

$$\Lambda_i(\omega) = \sum_n \sum_{m \in \mathbf{H}_i} |\langle \psi_n | m \rangle|^2 \delta(\omega - E_n), \quad (7)$$

where $|m\rangle$ represents the orthonormal basis of the subspace \mathbf{H}_i . We can identify the PES in Fig. 4(c) as follows: Λ_1 represents magnon sector, Λ_2 is related to one or more intra-site $D-Q$ transitions (SO excitons), Λ_3 and Λ_4 are the e-h continuum of $J_{eff} = 1/2$ states, and Λ_5 describes the e-h continuum of $J_{eff} = 3/2$ bands.

We notice intriguing features in Fig. 4(c): (i) Λ_1 and Λ_2 show the peaks in the range of $0 - 0.25$ and $0.5 - 1.0$ eV, respectively. These peaks are manifested in the RIXS spectra as the magnon and SO exciton bands. Λ_2 shows also the high energy peak at ~ 1.5 eV, which however does not directly couple to the RIXS process since it contains two SO excitons residing on different sites. (ii) Λ_3 and Λ_4 ($J_{eff} = 1/2$ e-h continuum) are located in the wide range of $0.5 - 1.5$ eV. This fact reveals that not only the lower but also the higher peak of $\sigma(\omega)$ is attributed to the e-h continuum of $J_{eff} = 1/2$ states, contrary to previous interpretation based on a simple band picture [2]. (iii) Λ_3 (NN e-h contribution) is depleted in the vicinity of the SO exciton Λ_2 . The mixing of these modes is natural in view of the nonzero overlap between quasi-degenerate $|ASDD\rangle \in \mathbf{H}_3$ and $|DQDD\rangle \in \mathbf{H}_2$ states [see Fig. 3(a,b)] by virtue of intersite hoppings.

The PES thus shows that the optically active e-h continuum of $J_{eff} = 1/2$ band and the optically forbidden SO exciton [S5] are located in the same energy range of $0.5 - 1.5$ eV, and there is considerable mutual interaction between these excitations due to the interband hopping between $J_{eff} = 1/2$ and $J_{eff} = 3/2$ states. Two peak structure in $\sigma(\omega)$ results from this unusual mixing among different excitations, which is reminiscent of the characteristic behavior of the Fano resonance.

To conclude, we presented a unified description of magnetic couplings, optical conductivity, and RIXS spectra in Sr_2IrO_4 within the model including strong SO coupling and ionic multiplet effects. The results obtained are consistent with the available experimental data. Since the SO splitting and the Mott-Hubbard charge gap are of similar scale, an unusual coupling between two different types of excitations – the optically inactive SO exciton and the optically active e-h continuum – is induced due to the interband mixing of $J_{eff} = 1/2$ and $J_{eff} = 3/2$ states. Although this effect is not very essential for NN magnetic interactions, it plays a crucial role in determining the shape of optical spectra: the e-h continuum is suppressed in the vicinity of the SO exciton inherent to iridates. The unusual Fano-type coupling between the rich ionic multiplet excitations and electronic continuum seems to be a characteristic feature of $J_{eff} = 1/2$ Mott insulators. This phenomenon is rooted to the atomic/band duality of $5d$ electrons and should therefore be generic to iridates with unusual hierarchy of energy scales.

We thank G. Jackeli for useful discussions. This work was supported by the NRF (No.2009-0079947).

* bimin@postech.ac.kr

- [1] M. Imada, A. Fujimori, and Y. Tokura, *Rev. Mod. Phys.* **70**, 1039 (1998).
- [2] B.J. Kim, H. Jin, S.J. Moon, J.-Y. Kim, B.-G. Park, C.S. Leem, J. Yu, T.W. Noh, C. Kim, S.-J. Oh, J.-H. Park, V. Durairaj, G. Cao, and E. Rotenberg, *Phys. Rev. Lett.* **101**, 076402 (2008).
- [3] S.J. Moon, H. Jin, K.W. Kim, W.S. Choi, Y.S. Lee, J. Yu, G. Cao, A. Sumi, H. Funakubo, C. Bernhard, and T.W. Noh, *Phys. Rev. Lett.* **101**, 226402 (2008).
- [4] B.J. Kim, H. Ohsumi, T. Komesu, S. Sakai, T. Morita, H. Takagi, and T. Arima, *Science* **323**, 1329 (2009).
- [5] H. Takagi (unpublished).
- [6] Y. Singh and P. Gegenwart, *Phys. Rev. B* **82**, 064412 (2010).
- [7] H. Watanabe, T. Shirakawa, and S. Yunoki, *Phys. Rev. Lett.* **105**, 216410 (2010).
- [8] C. Martins, M. Aichhorn, L. Vaugier, and S. Biermann, *Phys. Rev. Lett.* **107**, 266404 (2011).
- [9] R. Arita, J. Kuneš, A.V. Kozhevnikov, A.G. Eguiluz, and M. Imada, *Phys. Rev. Lett.* **108**, 086403 (2012).
- [10] J. Kim, D. Casa, M.H. Upton, T. Gog, Y.-J. Kim, J.F. Mitchell, M. van Veenendaal, M. Daghofer, J. van den Brink, G. Khaliullin, and B.J. Kim, *Phys. Rev. Lett.* **108**, 177003 (2012).
- [11] S. Fujiyama, H. Ohsumi, T. Komesu, J. Matsuno, B.J. Kim, M. Takata, T. Arima, and H. Takagi, *Phys. Rev. Lett.* **108**, 247212 (2012).
- [12] G. Jackeli and G. Khaliullin, *Phys. Rev. Lett.* **102**, 017205 (2009).
- [13] K. Ishii, I. Jarrige, M. Yoshida, K. Ikeuchi, J. Mizuki, K. Ohashi, T. Takayama, J. Matsuno, and H. Takagi, *Phys. Rev. B* **83**, 115121 (2011).
- [14] G. Khaliullin, W. Koshibae, and S. Maekawa, *Phys. Rev. Lett.* **93**, 176401 (2004).
- [15] L.J.P. Ament, G. Khaliullin, and J. van den Brink, *Phys. Rev. B* **84**, 020403(R) (2011).
- [16] S.J. Moon, Hosub Jin, W.S. Choi, J.S. Lee, S.S.A. Seo, J. Yu, G. Cao, T.W. Noh, and Y.S. Lee, *Phys. Rev. B* **80**, 195110 (2009).
- [17] N.N. Kovaleva, A.V. Boris, C. Bernhard, A. Kulakov, A. Pimenov, A.M. Balbashov, G. Khaliullin, and B. Keimer, *Phys. Rev. Lett.* **93**, 147204 (2004).
- [18] G. Khaliullin, P. Horsch, and A.M. Oleś, *Phys. Rev. B* **70**, 195103 (2004).
- [19] G. Khaliullin, *Prog. Theor. Phys. Suppl.* **160**, 155 (2005).
- [20] J. Kanamori, *Prog. Theor. Phys.* **30**, 275 (1963).
- [21] In the limit of $10Dq \rightarrow \infty$, the energy splitting between $j_{eff} = 1/2$ and $j_{eff} = 3/2$ is 1.5λ [12, 15]. At finite $10Dq$ values, however, this splitting increases: for $10Dq = 3.0$ eV, it is about 1.7λ .
- [22] S.J. Moon, M.W. Kim, K.W. Kim, Y.S. Lee, J.-Y. Kim, J.-H. Park, B.J. Kim, S.-J. Oh, S. Nakatsuji, Y. Maeno, I. Nagai, S.I. Ikeda, G. Cao, and T.W. Noh, *Phys. Rev. B* **74**, 113104 (2006).
- [23] J.C. Slater and G.F. Koster, *Phys. Rev.* **94**, 1498 (1954).
- [24] Beom Hyun Kim and B.I. Min, *New J. Phys.* **13**, 073034 (2011).
- [25] V.M. Katukuri, H. Stoll, J. van den Brink, and L. Hozoi, *Phys. Rev. B* **85**, 220402(R) (2012).
- [26] O.F. Schrimmer, A.Förster, H. Hesse, M. Wöhlecke, and S. Kapphan, *J. Phys. C* **17**, 1321 (1984).
- [27] See *Supplemental Material* for details.
- [28] H. Jin, H. Jeong, T. Ozaki, and J. Yu, *Phys. Rev. B* **80**, 075112 (2009).
- [29] This is because an average value of dipole matrix element $|\langle ASDD|\hat{J}_c|DDDD\rangle|^2$ is about ten times larger than, e.g., $|\langle ATDD|\hat{J}_c|DDDD\rangle|^2$.

SUPPLEMENTAL MATERIAL

The gap value and peak positions in optical spectra are most sensitive to the interaction parameters U and J_H . At the same time, there is large uncertainty concerning their values in iridates: current estimates for U (~ 2.2 eV [S1, S2], 3 eV [S3]) and for J_H (~ 0.2 eV [S2], 0.3 eV [S1], 0.6 eV [S3, S4]) vary broadly. We therefore determine U and J_H values such that they give a reasonable agreement with the observed optical gap and peak positions, and, at the same time, we cross-check them by calculating the magnetic exchange constants.

We found that $U \sim 2.2$ eV and $J_H \simeq 0.2 - 0.3$ eV suggested by Refs. [S1, S2] result in too large optical gap (see a representative curve in Fig. S1) and too small magnetic exchange constant J . Far better agreement with experiment is obtained when we slightly decrease U and substantially increase J_H (above 0.4 eV). Solid line in Fig. S1 shows the result for $U = 1.86$ eV and $J_H = 0.5$ eV. As discussed in the main text, this parameter set provides also the magnetic interactions and spin canting angles that are in fair agreement with experiment.

U and J_H can still be varied within the ranges 1.6-2.0 eV and 0.4-0.5 eV, respectively, with acceptable fit results concerning the optical data. For instance, we show in Fig. S1 the result for $U = 1.60$ eV and $J_H = 0.42$ eV (estimated as $J_H = 3B+C$ using the Racah parameters B and C for an octahedrally coordinated Ir^{4+} impurity [S6]). While these parameters provide optical spectra similar to that we found for $U = 1.86$ eV and $J_H = 0.5$ eV, the latter choice gives a magnetic coupling J which is closer to the observed value.

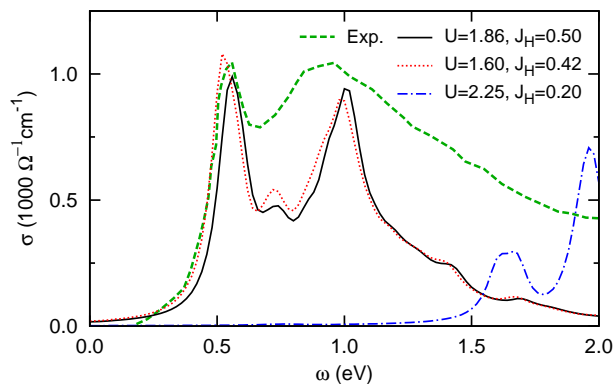


FIG. S1: (color online) Optical conductivity calculated with three different sets of U and J_H interaction parameters: $U = 1.86$ eV and $J_H = 0.50$ eV (solid line), $U = 1.60$ eV and $J_H = 0.42$ eV (dotted line), $U = 2.25$ eV and $J_H = 0.2$ eV (dashed-dotted line). Green dashed line represents the experimental data. The Heisenberg exchange couplings J calculated with these parameter sets are $J = 76.8$ meV, 83.0, and 37.8 meV, respectively; the experimental value is $J \simeq 60$ meV [S5].

* bimin@postech.ac.kr

- [S1] C. Martins, M. Aichhorn, L. Vaugier, and S. Biermann, Phys. Rev. Lett. **107**, 266404 (2011).
[S2] R. Arita, J. Kuneš, A.V. Kozhevnikov, A.G. Eguiluz, and M. Imada, Phys. Rev. Lett. **108**, 086403 (2012).
[S3] R. Comin, G. Levy, B. Ludbrook, Z.-H. Zhu, C.N. Veenstra, J.A. Rosen, Yogesh Singh, P. Gegenwart, D. Stricker, J.N. Hancock, D. van der Marel, I.S. Elfimov, A. Damascelli, arXiv:1204.4471.
[S4] D. van der Marel and G.A. Sawatzky, Phys. Rev. B **37**, 10674 (1988).
[S5] J. Kim, D. Casa, M.H. Upton, T. Gog, Y.-J. Kim, J.F. Mitchell, M. van Veenendaal, M. Daghofer, J. van den Brink, G. Khaliullin, and B.J. Kim, Phys. Rev. Lett. **108**, 177003 (2012).
[S6] B. Andlauer, J. Schneider, and W. Tolksdorf, Phys. Stat. Sol. B **73**, 533 (1976).